17th Australasian Fluid Mechanics Conference
Auckland, New Zealand
5-9 December 2010

# Cold Modelling of Two Phase Separation in a Rotary Holding Furnace

**A.S. Burrows[1], J.L. Liow[2*] and K. Brady[3]**

[1]Xstrata Technology, Level 2, 87 Wickham Terrace
Brisbane, Queensland, 4000 Australia

[2]School of Engineering and Information Technology
UNSW@ADFA, Canberra, ACT, 2600 Australia

[3]H 897 RSD Invermay, Victoria, 3352 Australia

## Abstract

A cold model of a rotary holding furnace was studied using water and a kerosene-LIX®973N organic mixture which are immiscible. The residence time distribution obtained showed that there was an optimum depth of the upper layer of organic where mixing with the bath fluid was maximised. The use of air bubblers showed that at low air flow rates, the air curtain acted to limit mixing but as the air flow rates increased, the circulation caused by the air flow increased mixing. The flow of the feed was found to behave similar to a gravity current where the feed preferentially moved along the liquid-liquid interface.

## Introduction

In the Isasmelt process for copper smelting, copper ores are reacted with oxygen and silica to form a two phase liquid mixture of copper matte and slag in the Isasmelt furnace (Errington *et al.* [2]). This mixture is then settled in a rotary holding furnace (RHF) where the mixture is fed in at one end and exits through side ports close to the opposite end of the furnace. The shape of the RHF is a long circular cylinder lying on its side and sits on a set of rollers (figure 1). The rollers enable the RHF to partially rotate about its axial axis to allow the copper matte and slag to be poured out through exit ports that are located at opposite ends of the circumference. The high temperatures and corrosive nature of the mixture does not allow the feed to be fed at the interface of the two fluids as is commonly found in mixer-settler equipment. Instead, it is poured into the RHF through a chute onto the surface of the molten fluid and then allowed to separate out with the contents tapped at convenient intervals depending on the downstream processes. Matte is often entrained in the slag layer and results in the loss of copper when the slag is disposed.

The loss of copper in slag is not well understood although it is often claimed that the loss is dominated by chemical equilibrium. Equilibrium studies however show that the loss is limited to 0.4–0.6%Cu in slag while plant studies indicate the %Cu in slag varies from 0.6 to 2% [1]. This large variation is attributed to physical entrainment but there has been no systematic study of the flow in a RHF. Possible causes for the entrainment suggested by plant operators include the rotation of the RHF during slag and matte tapping, feed occurring while the slag is being tapped, variation in the slag layer thickness and the operation of the gas bubblers made from porous plugs. During operation, the matte is tapped whenever the converters require a matte feed. The vagaries of the matte tapping results in varying levels of the slag layer and it has been noted that the copper content in the slag varies with the frequency and rate of matte tapping. As the slag depth varies with fill, the residence times and flow characteristics of the slag layer changes, which in turn can affect the coalescence and settling of the matte. However, little is known of the flow characteristics and residence time distribution as it is difficult to study them under the severe conditions present in the RHF.

*Corresponding author

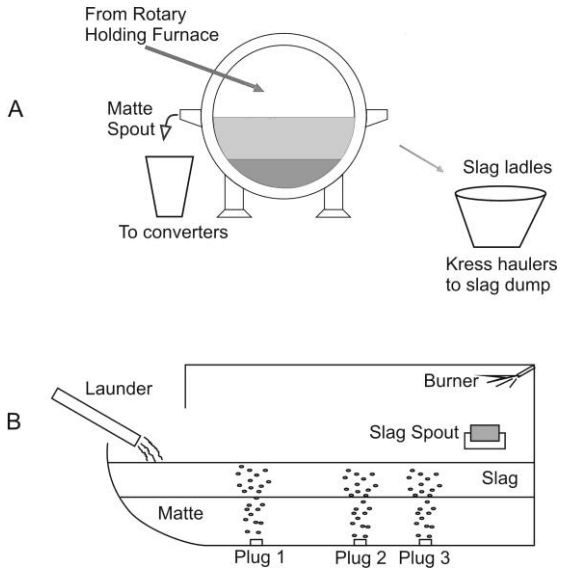


Figure 1. A: Cross section of the rotary holding furnace showing the matte and slag spouts. B: Axial length showing feed launder and outlet positions.

In this study a cold model of the RHF was used to investigate the flow behaviour through residence time modelling of the feed to the slag spout and the effect of varying the slag layer thickness. A number of dimensionless numbers are important, including the Reynolds, Froude, and Weber numbers as well as the Galileo number representing the physical properties of the fluids.

## Experimental

The use of a cold model required parameters to be matched. The physical properties of the matte-slag system are tabulated in table 1. The cold model was a PMMA 1/10th scale model of the plant equipment at Mount Isa.

### Choice of fluids

Attempting to ensure dynamic similarity and select a convenient tracer resulted in two constraints that were difficult to satisfy. The density ratio, volumetric flow-rate ratio and Galileo numbers were reasonably satisfied but it was not possible to match the viscosity ratios as shown in table 2. The matte was modelled with water while the slag was modelled with a 30%v/v organic

solution of LIX® 973N solvent extractant in kerosene. LIX® 973N comprises of 46 vol% nonylsalicyl aldoxime, 18% ketoxime, 6% nonylphenol and 30% diluent and is a copper extractant used in hydrometallurgy. Copper is soluble in LIX® 973N and changes to a dark brown colour that progressively gets darker with increasing concentrations of copper. The properties of the organic solution are given in table 1 and show only a small variation between the maximum and minimum values of copper loading.

| | Density ($kg/m^3$) | Viscosity (kg/ms) | Surface tension (N/m) |
|---|---|---|---|
| Matte (~1200°C) | $4.7\times10^{3}$ | 0.01 | 0.33 |
| Slag (~1200°C) | $4.7\times10^{3}$ | 0.40 | 0.41 |
| Water (20°C) | 997 | $1.00\times10^{-3}$ | 0.073 |
| Kerosene (20°C) | 783 | $1.20\times10^{-3}$ | 0.026 |
| 30% v/v LIX 973N in kerosene with 85 mg/l Cu | 828 | $2.90\times10^{-3}$ | 0.023 |
| 30% v/v LIX 973N in kerosene with 480 mg/l Cu | 831 | $3.05\times10^{-3}$ | 0.022 |

Table 1. Physical properties of the matte and slag in the RHF and the cold model liquids.

| | Mt Isa RHF | Cold model |
|---|---|---|
| Upper liquid flowrate ($L_1$) | 50 tph | 420 ml/min |
| Volumetric flowrate ratio ($L_1$:$L_2$) | 6:4 | 7:3 |
| $N_{Re}(L_1) = ud/\nu$ | 9.6 | 5.5 |
| $N_{Fr}(L_1) = u^2/gd$ | $1.9\times10^{-6}$ | $6.3\times10^{-7}$ |
| $N_{Ga}(L_1) = gd^3/\nu^2$ | $4.8\times10^{7}$ | $4.8\times10^{7}$ |
| Density ratio $L_1$:$L_2$ | 0.74 | 0.83 |
| Viscosity ratio $L_1$:$L_2$ | 40 | 3 |

Table 2. Dynamic similarity comparisons between the RHF and the cold model.

Fluid viscosities were measured with a Brookfield DVII+ viscometer, surface tension was measured by the capillary rise technique, and interfacial tension measured by the pendant drop technique. The interfacial tension between the organic and water showed a dynamic surface tension that varied between 0.0197 N/m at the start to 0.0182 N/m after 10 minutes with the pendant drop technique. The interfacial tension stabilised after 10 minutes but the small variation is not expected to affect the flow characteristics although it may have an effect on the coalescence of droplets and settling of the liquid phases [3].

## Experimental setup

Figure 2 shows a schematic of the cold model. The water was kept at a neutral pH to ensure that the copper tracer remained in the organic phase and maintained at 20°C with a heater. The organic-water mixture was emulsified with a perforated 30 mm diameter disc PMMA impeller of 3mm thickness in a 50 mm diameter fully-mixed mixing chamber. An Analite SU1 electric stirrer operating at 600 rpm was used to provide a consistent shear rate for all the runs. The mixture was then fed directly onto the free surface of the liquid in the RHF model at a flow-rate of 420 ml/min of organic and 120 ml/min of water. At the start of the experiment, the flow was allowed to stabilise for 1.5 residence time before a step change in the copper concentration was introduced in the organic phase. Following the step change in feed concentration, 30 to 33 samples of the organic phase were taken periodically at the outlet.

The samples were diluted with 9 parts kerosene to 1 part sample prior to analysis with a GBC 902 atomic absorption spectroscope (AAS) to ensure the samples fell within the analysis range and to reduce viscosity variations between samples. AAS standards were used for calibrating the copper and a straight line fit was obtained for Cu concentration against absorbance. The Cu concentration error was within 1% giving the dimensionless concentration ($F(\theta)$) error of ~2%.

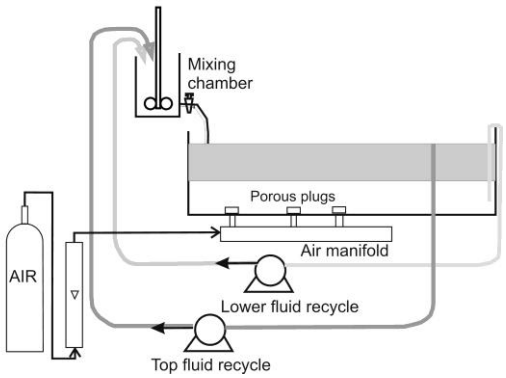


Figure 2. Schematic of the cold model.

A series of runs were made where the depth of the upper liquid layer was varied from 18.5 mm to 48 mm. A few runs were then run with an upper liquid layer depth of 37.5 mm with the air bubblers providing air flow rates ranging from 1.5 to 5.0 l/min to see if the presence of an air plume affected the mixing and residence time of the upper layer. A few repeats were carried out (*e.g.* C29 in table 3 was repeated 3 times) and showed that the results were reproducible and the greatest discrepancies occurred at $\theta>1.5$ where the contribution of the *F*-curve to the results is not significant.

## Modelling

The copper concentration measured in the slag spout to a step change in copper concentration gives the *F* curve of the downstream signal. A typical *F* curve is shown in figure 4 and it exhibits an S-shaped curve indicating dispersion of the feed in the cold model. The curve rises quite sharply between the dimensionless times of 0.5 to 1.0 suggesting that the curve can be modelled with a finite number ($n$) of fully mixed reactors occupying a fraction ($b$) of the total volume. There is a short time lag between the introduction of the change in feed concentration and its emergence at the outlet and this indicates that a significant plug flow exists which occupies a fraction ($p$) of the total volume, hence $b+p \le 1$. It is also expected that there is some dead volume as the outlet is not located at the opposite end of the cold model. Any dead volume in the system will be the total volume minus the volume occupied by the mixed and plug flow reactors, *i.e. 1-b-p*. The outlet concentration or the *F* curve for this model is given by [4]

$$F(\theta) = \begin{cases} 0 & \text{for } 0 \le \theta \le p \\ 1 - \left[ e^{-\frac{n}{b}(\theta - p)} \right] \times \sum_{j=1}^{j=n} \frac{\left[ n/b (\theta - p) \right]^{j-1}}{(j-1)!} & \text{for } \theta > p \end{cases} \quad (1)$$

The model was fitted to the experimental data to obtain values for $n$, $b$ and $p$, where $n$ is restricted to integer values. The value of $F(\theta)$ is the dimensionless concentration for an input stream undergoing a step change from $C_0$ to $C_\infty$ and is given by

$$F(\theta) = \frac{C - C_0}{C_\infty - C_0} \quad (2)$$

## Results

### Observations

The feed stream entering the cold model contains an emulsion of organic and water. The feed mixture entrains some air as it enters the cold model and its momentum propels it initially to penetrate the lower water layer as a jet. It then rises back to the liquid-liquid interface before spreading out. As time progresses, the depth of penetration of the feed stream into the water layer decreases while the colour of the upper organic layer becomes lighter. This is due to the entrainment of water drops into the organic layer that only disengages after the flow has moved further down the cold model resulting in the organic layer near the feed end increasing in density. The step change in concentration was carried out only after a steady state of the jet penetration depth was observed.

Following introduction, the fresh feed travels along the liquid-liquid interface as a gravity current. Initially, the feed spreads out radially but after reaching the side walls it travels axially down the model with a parabolic shaped front (figure 3). When it reaches the outlet, part of the feed flows out of the model but a portion continues towards the sealed end of the model. The parabolic profile gets progressively more distorted towards the outlet side as the feed front travels down the model.

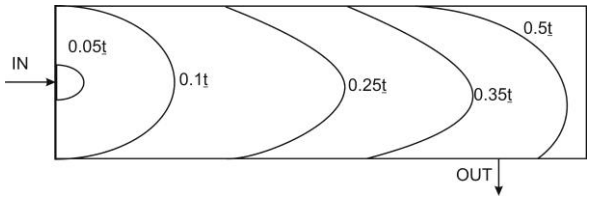


Figure 3. Flow profiles at five dimensionless times after a kerosene-LIX step input.

The steady stable flow patterns within the organic layer required an initial period to settle down. This occurred only if the organic and water feed was thoroughly emulsified prior to its introduction. Feeding unmixed water and organic concurrently through the same nozzle led to instabilities where the fresh feed often short-circuited the organic layer by flowing along a narrow channel on one side of the model to the exit. This set up recirculation zones in the bulk of the cold model so that it was not possible to carry out residence time modelling without emulsifying the feed thoroughly.

### *F* curves

The *F*-curves are shown in figures 4 and 5 for six different depths of the upper liquid layer. They model the extent of mixing as the depth of the slag layer is increased, which often occurs when the lower layer of matte is rapidly removed. In the range of 30 to 37.5 mm upper liquid layer depth as shown in figure 4, the *F*-curves show a noticeable broadening as the upper liquid layer depth increases indicating that the amount of mixing has increased. The step change also appears earlier as the upper liquid layer depth increases. The curves intersect around a dimensionless time of 0.75 with an *F*-value of 0.36.

In contrast, the *F*-curves for an upper liquid layer depth in the range of 37.5 to 48 mm, plotted in figure 5, show a narrowing as the depth increases. As the depth increases, the *F*-curves get steeper but after a dimensionless time of about 1.5, the *F* values begin to change much more slowly resulting in a long tail. This tail is caused by the increased volume where the feed can mix before exiting. The separation between the curves for dimensionless times greater than 1 is more obvious than that of figure 4 which may suggest more of the flow is bypassing preferentially to the exit as the depth increases. The *F*-curves show that the mixing is affected by the depth of the upper liquid layer and there exists a maximum in the amount of mixing as a function of the depth of the upper liquid layer. The curves also intersect similar to figure 4, around a dimensionless time of 0.75 with an *F*-value of 0.36.

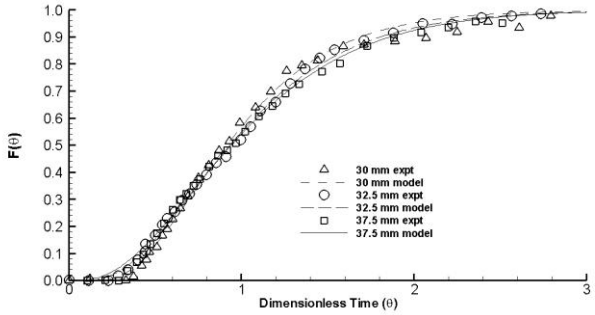


Figure 4. *F*-curves for upper liquid layer depths between 30 to 37.5 mm

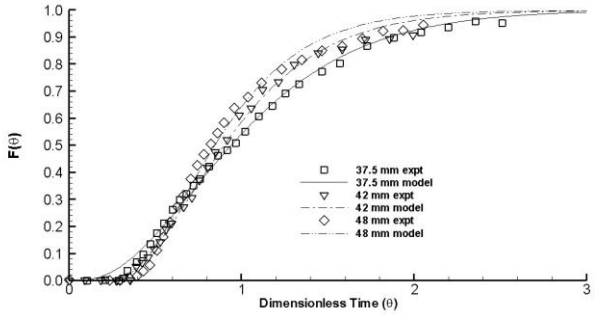


Figure 5. *F*-curves for upper liquid layer depths between 37.5 to 48 mm.

Figure 6 shows the *F*-curves for different air bubbler flow rates. When the air flow is initially introduced it results in a sharp reduction in mixing as the air bubblers compartmentalise the cold model. As the air flow rate is increased, the curves broaden progressively resulting in increased mixing. Surprisingly, the air bubbling results in less mixing compared to the case without air bubbling.

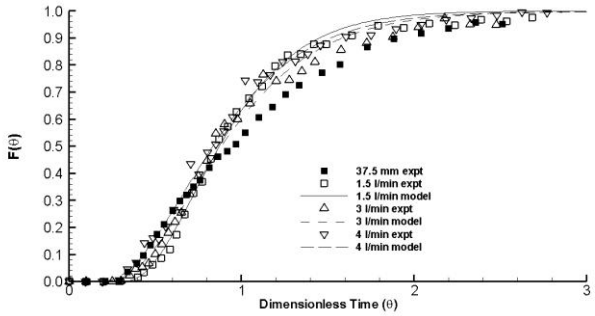


Figure 6. *F*-curves for a upper liquid layer depths of 37.5 mm but with different air flow rates. The filled square is without air bubbling.

### Fitting of the model

The model was fitted by constraining the value of *n* to take only integer values. The values of *b* and *p* were then optimised with a non-linear curve fitting routine in Maple. The optimum value of *b* and *p* required both minimisation of the sum of squares of the error of fit as well as ensuring that $b+p$ was as close to 1 as possible, The sum of $b+p$ is dependent on the accuracy of the results which is estimated to be of about ±5% based on the accuracy of the analysis, flow rates, and control of the depth of

the layers. Table 3 lists the runs and the values from curve fitting. The sum of $b+p$ has a maximum value of 1.05 for the case of a 37.5 mm upper liquid layer depth but is still within the accuracy of the results. As each run takes over a week to complete with the analysis, only a few were repeated but are not reported here.

| No | Feed-rate, l/min | Upper layer depth, mm | Air flow rate, l/min | *n* | *b* | *p* |
|---|---|---|---|---|---|---|
| C22 | 0.42 | 25.5 | 0 | 3 | 0.600 | 0.313 |
| C24 | 0.42 | 30.0 | 0 | 3 | 0.871 | 0.135 |
| C23 | 0.43 | 32.5 | 0 | 3 | 0.981 | 0.054 |
| C29 | 0.45 | 37.5 | 0 | 3 | 1.042 | 0.013 |
| C25 | 0.44 | 42.0 | 0 | 3 | 0.821 | 0.016 |
| C35 | 0.43 | 46.0 | 0 | 3 | 0.733 | 0.240 |
| C33 | 0.43 | 48.0 | 0 | 3 | 0.725 | 0.196 |
| C36 | 0.44 | 38.0 | 1.5 | 3 | 0.656 | 0.288 |
| C27 | 0.43 | 37.0 | 3.0 | 3 | 0.790 | 0.174 |
| C37 | 0.43 | 38.5 | 4.0 | 3 | 0.767 | 0.146 |

Table 3. Summary of the runs conducted.

## Discussion

The accuracy of the experiments is strongly affected by the accuracy in measuring the concentration of the copper in the samples. In particular, towards the tail of the F-curves, the changes in concentration are small and small changes are exacerbated. Furthermore, the experiment was not carried out for more than 3 dimensionless times as the number of samples obtained became excessive and there was a limit to the amount of emulsion available for the run. The value of $b+p$ can also be estimated from the area between $F(\theta)=1$ and the $F$ curve by integrating equation (1) and the $b+p$ values obtained are similar to those obtained by curve fitting and can exceed 1. This indicates that the errors are inherent in the experimental data and not in the curve fit.

The interfacial tension was found to change with time but it is not clear how the dynamics of the flow is affected by the interfacial tension. The coalescence rate of droplets in an aqueous-organic emulsion is usually decreased as the interfacial tension increases [3] but the change measured for the water-organic is only 0.0015 N/m. Nevertheless, it was found that when the feed was not emulsified, significant bypassing of feed to the outlet resulted.

There is mixing of the feed stream with the contents in the cold model which is shown by the low value of $n=3$. The variance is proportional to $1/n$ and the graphs show that more than half of the feed exits before the one mean residence time. The bypassing of the feed to the outlet can be seen in figure 3 where the organic layer progressively favours a path towards the exit side. For low upper liquid layer depths, there is a tendency for a larger dead volume to be present. This can be accounted for by the fact that the feed stream will preferentially flow towards the outlet as the outlet was a PVC pipe of 8 mm in diameter, a size similar to the upper liquid layer depth. As the liquid layer gets deeper, the flow of the upper liquid layer will have to converge into the outlet pipe diameter and liquid that is further away from the pipe centreline will have a smaller driving force to flow into the pipe and will instead preferentially flow towards other parts of the cold model. It was observed that at low upper liquid layer depths, there is evidence of stringing towards the outlet pipe, where the feed forms strings or fingers that accelerate away from the bulk of the feed and move towards the outlet pipe forming strings of darker fluid. This stringing effect disappears when the upper liquid layer depth was increased above 30 mm.

The interface layer formed at the liquid-liquid interface was found to travel the fastest, usually moving ahead of the rest of the organic layer above it. The velocity of this front decreases with distance and behaves similar to a gravity current. However as the organic and water droplets separate, the front slowly lightens and its velocity slows down. Nevertheless, for all runs, the interfacial layer still reached the outlet position faster than the rest of the feed fluid.

The upper liquid layer depth also shows an optimum value for mixing, and this is most likely due to the interaction between the outlet pipe diameter, the thickness of the upper liquid layer and the flow profile near the outlet region. For small upper liquid layer depth, there is limited opportunity for the liquid to mix vertically. As the liquid depth increases there is a tendency for the flow to begin mixing vertically forming recirculating zones as well as moving further towards the closed end of the cylinder. This in turn will give rise to the long tail in the $F$ curve that is indicative of regions that are relatively stagnant and cause a hold-up of the original feed mixture. This is supported by the dead volumes for the 46 and 48 mm upper liquid layer depths being 2.7% and 7.9% respectively.

The results clearly show that the fluid flow in the cold model is influenced not only by the flow patterns but also by the possibility of flow stratification within the layers. The dominant behaviour depends on the depth of the upper fluid layer and the method in which the feed is prepared prior to introduction into the model. In the RHF, the feed is normally well mixed due to the intense mixing that occurs in the Isasmelt prior to feeding into the RHF. However, as stratification of the feed and variations in the flow behaviour depends on the thickness of the upper layer, it may be important to control the thickness of the slag layer to prevent bypassing of matte into the slag spout resulting in loss of copper before the matte can settle down into the lower matte layer.

## Summary and Conclusions

A study of the residence time distribution in an axially positioned cylinder for the settling of an emulsion of two immiscible liquids showed that mixing is dependent on the depth of the upper liquid layer. The residence time distribution could be reasonably modelled by a three fully mixed reactors and a plug flow reactor in series. As the upper liquid layer increased, the flow behaviour becomes more complex and an increased tendency for mixing with the bulk of the fluid in the cold model resulting in a long tail for the exit concentration. The use of air bubblers was found not to improve mixing, rather it split the cylinder's interior into separate compartments and reduced mixing.

## Acknowledgments

A. S. Burrows acknowledges the financial support of MIM Ltd.

## References

[1] Burrows, A. S. *Copper loss into rotary holding furnace slag*. MApplSci thesis, University of Ballarat, 1999.

[2] Errington, W. J., Edwards, J. S., & Hawkins, P., Isasmelt technology - current status and future development. *J SAIMM.*, **97**, 1997, 161-167.

[3] Jeffreys, G.V., Davies, G.A. & Pin, K., Rate of coalescence of the dispersed phase in a laboratory mixer-settler unit: Part II, The analysis of coalescence in a continuous mixer-settler. *AIChE J.*, **16**(5), 1970, 827-831.

[4] Wolf, D. & Resnick, W., Residence time distribution in real systems, *I&EC Fund.*, **2**, 1963, 287-293.